Nonlinear Compensator Design for Active Sliders to Suppress Head-Disk Spacing Modulation in Hard Disk Drives

Jia-Yuang Juang, *Student Member, IEEE*, and David B. Bogy, *Fellow, IEEE*

***Abstract*—As the slider's flying height (FH) continues to reduce in hard disk drives, the flying height modulation (FHM) due to disk morphology and interface instability caused by highly nonlinear attractive forces becomes significant. Based on the concept that the FH of a portion of the slider that carries the read/write element can be adjusted by a piezoelectric actuator located between the slider and suspension and that the FH can be measured by the use of the magnetic readback signal, a new 3-DOF analytic model and an observer-based nonlinear compensator are proposed to achieve ultralow FH with minimum modulation under short-range attractive forces. Numerical simulations show that the FHM due to disk waviness is effectively controlled and reduced.**

***Index Terms*—Air-bearing slider, flying height modulation (FHM), hard disk drives, head-disk interface (HDI), intermolecular and electrostatic forces, observer-based sliding mode control.**

I. Introduction

THE areal density of magnetic recording in hard disk drives has been increasing at a rate of 1.6 times per year since the 1990s. This achievement has been enabled mechanically by decreasing the distance between the read/write transducer and the rotating disks. According to the Wallace spacing loss equation, the magnetic signal strength increases exponentially as the distance decreases between the magnetic media and the transducer. Therefore, the maximum magnetic signal can be potentially obtained at a spacing of zero, resulting in a contact recording scheme. However, when the slider comes into contact with the disk, other considerations must be addressed to assure a stable contact interface with minimum wear and contact bouncing vibration.

As the flying height (FH) is reduced in a flying head slider to the sub-3-nm regime in ultrahigh density hard disk systems, the flying height modulation (FHM) induced by the disk morphology and dynamic instability due to short-range attractive forces become more significant. Gupta and Bogy [1] conducted a numerical study on the effect of intermolecular and electrostatic forces on the stability of the head-disk interface (HDI), and they showed that those short-range attractive forces may cause an instability of the HDI at such low FHs. This effect must be considered in the design of air-bearing surface (ABS).

Manuscript received October 26, 2004; revised July 22, 2005. Recommended by Technical Editor Bleuler. This work was supported by the Computer Mechanics Laboratory (CML), University of California, Berkeley, and the work of J. Y. Juang was supported by the California State Nanotechnology Fellowship.

The authors are with the Computer Mechanics Laboratory, Department of Mechanical Engineering, University of California, Berkeley, CA 94720 USA (e-mail: jiayang@me.berkeley.edu).

Digital Object Identifier 10.1109/TMECH.2006.875563

To achieve reliable reading and writing of magnetic data, it is required that the transducer location on the slider vibrate less than $\pm 10\%$ of the nominal FH, or about ± 0.3 nm in future systems for 1 Tbit/in^2 areal density. Furthermore, considerable FHM may cause instability of the interface due to adhesive forces. The concept of FH adjustment by piezoelectric material has been proposed in [2]–[4], where the main purpose was to decrease the effects of manufacturing tolerances and environmental variations on the FH. The authors utilized silicon microfabrication technology to fabricate the sliders. However, the use of silicon as the slider material may cause other issues in slider fabrication and HDI tribology. Li *et al.* [5] presented a real-time FH detection method by using readback or thermal signals, and in [6], they developed a real-time feedback control method to suppress the FHM. In this case, the actuator was a piezoelectric film attached to the suspension. The actuation bandwidth was limited by the suspension dynamics. The effect of short-range attractive forces was not taken into consideration in their study.

In this paper, a novel controlled flying proximity (CFP) slider is presented. A new 3-DOF analytic model is proposed to characterize the dynamics of the piezoelectric-actuated slider. The air-bearing parameters, such as stiffness and damping, are identified by a modal analysis method developed in the Computer Mechanics Laboratory (CML) [7], [8]. Then, an observer-based nonlinear sliding mode controller [9] is designed to compensate the short-range attractive forces and to suppress the FHM of ultralow FH air-bearing sliders in proximity, in which the magnetic signal is used for real-time FHM measurement. The attractive forces are included in the model as a highly nonlinear term and the effect of disk morphology is modeled as an unknown but bounded disturbance. The performance of the controller is investigated here by numerical simulations.

II. Air-Bearing Slider Dynamics

An air-bearing slider dynamic response is obtained by simultaneously solving the generalized Reynolds equation to attain the pressure distribution over the ABS and the equations of motion characterizing the rigid body motion of the slider body

$$\frac{\partial}{\partial x}\left(ph^3Q\frac{\partial p}{\partial x}\right)+\frac{\partial}{\partial y}\left(ph^3Q\frac{\partial p}{\partial y}\right)=6\mu U\frac{\partial}{\partial x}(ph)+6\mu V\frac{\partial}{\partial y}(ph)+12\mu\frac{\partial}{\partial t}(ph)$$

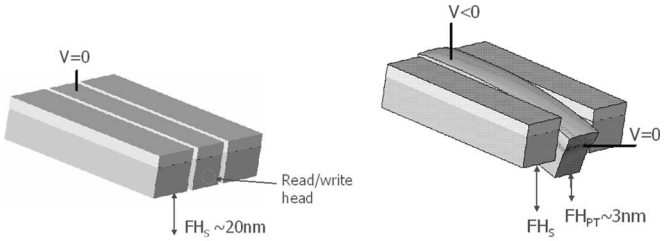

(a) Passive mode (no control is applied) (b) Active mode (control is applied)

Fig. 1. Two operational modes of a CFP slider with PZT actuation. The read/write head is not shown.

$$m\ddot{z} = F_{\rm s} + \int_A (p - p_{\rm a})\, dA$$

$$I_\theta \ddot{\theta} = M_{{\rm s}\theta} + \int_A (p - p_{\rm a})(x_{\rm g} - x)\, dA$$

$$I_\phi \ddot{\phi} = M_{{\rm s}\phi} + \int_A (p - p_{\rm a})(y_{\rm g} - y)\, dA$$

where p is the pressure; h is the local slider-disk spacing; μ is the viscosity of the air; Q is the flow factor; U and V are the relative velocities in the x- and y-directions between the slider and disk; $p_{\rm a}$ is the ambient pressure; and $x_{\rm g}$ and $y_{\rm g}$ are the positions of the slider's center of gravity; $F_{\rm s}, M_{{\rm s}\theta}$, and $M_{{\rm s}\phi}$ are the force and moments applied by the suspension in the z-, θ-, and ϕ-directions; and I_θ, I_ϕ, and m are the moments of inertia and mass of the slider, respectively. Simultaneously, satisfying these equations gives the slider's dynamic response in the vertical (z), pitch (θ), and roll (ϕ) DOFs to various excitations. The above equations are highly nonlinear. The CML dynamic simulator was developed to numerically solve this set of equations. The solutions are accurate but the time-consuming computation makes it difficult to use the simulator as the system in our compensator design. In this paper, a lumped parameter analytic model was used to serve as the plant. The parameters, such as stiffness and damping, were identified by a modal analysis method. This approach gives accurate solutions and requires much less computation.

III. Nonlinear 3-DOF-Lumped Parameter Model of CFP Sliders

A schematic diagram of the CFP slider is shown in Fig. 1. The FH is about 20 nm in the off-duty cycle and is reduced to about 3 nm during reading and writing. Fig. 2 shows the five-pad ABS design example used in this paper. The pole tip FH $(\mathrm{FH_{pt}})$ is adjusted by the deflection of the cantilever actuator. The deflection is achieved by grounding the slider and applying a negative voltage to the top electrode of the central piezoelectric layer.

There are two modes of operation. In the passive mode, there is no external voltage applied to the piezoelectric layer, and so the active cantilever rests in the undeflected position. The $\mathrm{FH_{pt}}$ in this case may be designed to be anywhere between 10 and 20 nm, depending on the ABS design. In the active mode, the cantilever is bent into close proximity of the disk with the application of a negative dc voltage to the middle portion of the piezoelectric material. Meanwhile, an ac-computed control voltage is superposed on the dc voltage so that the FHM is minimized. The active mode is used only when the read/write head is in operation. The duty cycle for a practical head is rather low, as most of the time of the head is spent on nonread/nonwrite actions, such as latency, seeking, or idle. Thus, the wear and power consumption can be greatly reduced by simply operating the CFP in the passive mode. The air-bearing pressure distributions in both modes are shown in Fig. 3, where the additional pressure peak is seen in Fig. 3(b) when the central pad is deflected into close proximity to the disk.

As shown in Fig. 4, the CFP slider is modeled as a nonlinear 3-DOF-lumped parameter model in which the cantilever actuator and the air-bearing dynamics are modeled as 1-DOF and 2-DOF, respectively.

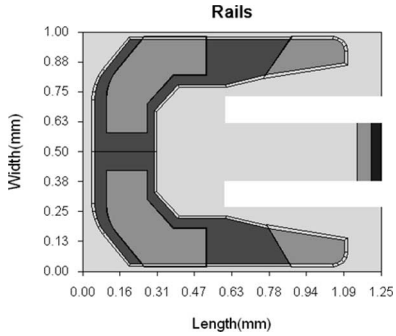

Fig. 2. ABS design of the CFP slider.

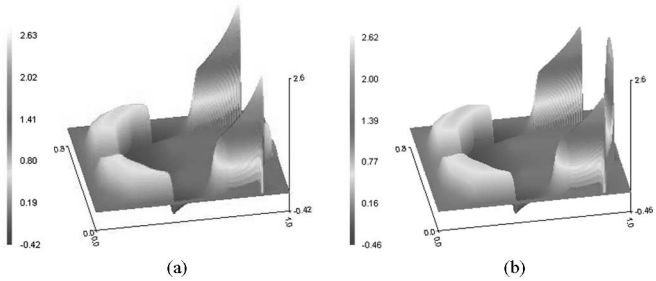

Fig. 3. Air pressure distributions of the ABS in Fig. 2. (a) Passive mode and (b) active mode. The pole tip FH has been reduced from 20 to 2.35 nm.

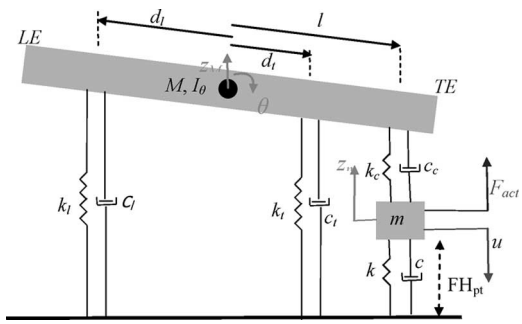

Fig. 4. 3-DOF dynamic model of CFP sliders.

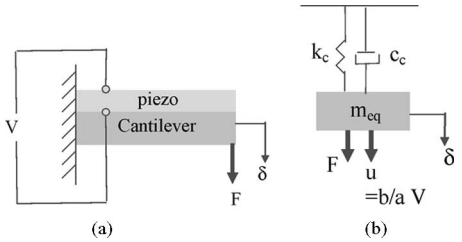

Fig. 5. (a) Piezoelectric composite beam actuator and (b) the 1-DOF model.

A. 1-DOF-Lumped Model of the Piezoelectric Cantilever Actuator

The cantilever actuator, composed of a piece of piezoelectric material and a cut-out portion of the slider, deflects under an electric voltage V and an external vertical force F exerted on the tip as shown in Fig. 5(a). V and F are the control voltage and air-bearing force in our application. The constitutive equations that determine the tip deflection subject to a voltage and a force can be described as follows [10]:

$$\begin{aligned}\delta &= aF + bV \\ a &= \frac{1}{k_c} = \frac{4L^3}{E_p w t_p^3} \frac{\alpha\beta(1+\beta)}{\alpha^2\beta^4 + 2\alpha(2\beta + 3\beta^2 + 2\beta^3) + 1} \\ b &= \frac{3L^2}{t_p^2} \frac{\alpha\beta(1+\beta)}{\alpha^2\beta^4 + 2\alpha(2\beta + 3\beta^2 + 2\beta^3) + 1} d_{31} \\ \alpha &= E_s/E_p \quad \beta = t_s/t_p \end{aligned} \tag{1}$$

where the subscripts s and p stand for the slider and piezoelectric materials, respectively, E and t are the Young's modulus and beam thickness, respectively, L and w represent the length and width of the composite beam, k_c is the bending stiffness of the cantilever, and d_{31} is the piezoelectric coefficient.

The deflections of the cantilever for three different slider thicknesses (0.3, 0.23, and 0.2 mm) under 1 V (without external force) were calculated according to (1) and were also simulated by a finite element analysis (FEA) with the results as shown in Fig. 6. It was found that an optimal thickness of the PZT exists for which the deflection is maximized for a given voltage and slider thickness.

According to (1), the cantilever is modeled as a 1-DOF mass-damper-spring system with (bending) stiffness k_c and damping c_c as shown in Fig. 5(b). k_c is determined by (1) and c_c is assumed to be zero in the calculation. The equivalent mass m_{eq} is calculated by the following equation:

$$m_{eq} = \frac{k_c}{\omega_n^2} \tag{2}$$

where ω_n is the first natural frequency of the cantilever obtained by the FEA. ω_n is about 3.380×10^6 rad/s for a pico-sized CFP slider with 300 μm thickness and 80 μm PZT plate as shown in Fig. 7. Since the bandwidth of the PZT itself is very high, the bandwidth of the cantilever actuator is primarily limited by the first resonant frequency of the structure, i.e., about 500 kHz in this case.

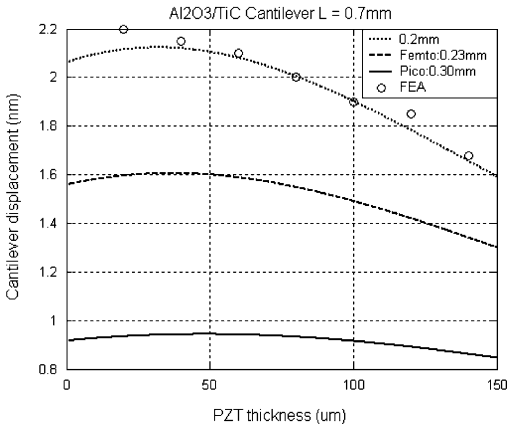

Fig. 6. Deflection of the cantilever tip under 1 V. The solid line is for a pico-slider thickness, the dash line is for the femto slider thickness. FEA shows the following results carried out: $E_p = 62$ GPa, and $E_c = 398$ GPa, and $d_{31} = -360 \times 10^{-12}$ m/V.

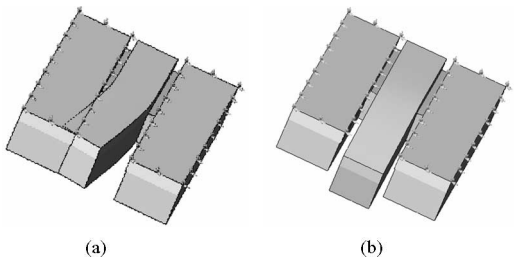

Fig. 7. First two modes of a pico-sized CFP slider simulated by FEA (COSMOSDesignSTAR). The natural frequencies are 538 and 550 kHz (Slider thickness $= 300$ μm, PZT thickness $= 80$ μm). (a) The first mode (in plane) and (b) the second mode (out of the plane).

B. 2-DOF-Lumped Parameter Model of the Air Bearing and Its Parameter Identification

In this section, we focus on the air-bearing dynamics while the cantilever is fixed, i.e., without moving relative to the rest of slider. For symmetric ABS designs and flying at 0° skew, the motion of the slider in the roll direction makes little contribution to the system response. However, the two pitch modes contribute to the slider's dynamics at the R/W transducer. This can be modeled as a 2-DOF system as shown in Fig. 8(a). The equation of motion of this model for free vibration can be expressed in the following form:

$$[m]\{\ddot{x}\} + [c]\{\dot{x}\} + [k]\{x\} = \{0\} \tag{3}$$

where

$$\{x\} = \begin{bmatrix} z_M \\ \theta \end{bmatrix} \quad [m] = \begin{bmatrix} M & 0 \\ 0 & I_\theta \end{bmatrix}$$

$$[c] = \begin{bmatrix} c* + c_l & -(d_t c* - d_l c_l) \\ -(d_t c* - d_0 c_l) & d_t^2 c* + d_l^2 c_l \end{bmatrix}$$

$$[k] = \begin{bmatrix} k* + k_l & -(d_t k* - d_l k_l) \\ -(d_t k* - d_l k_l) & d_t^2 k* + d_l^2 k_l \end{bmatrix}$$

in which z_M and θ are the displacement of the slider's mass center and the pitch angle of the slider with zero mean values,

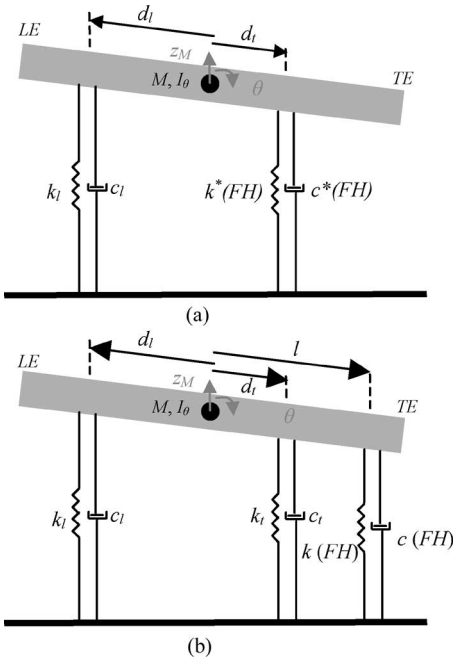

Fig. 8. Schematic diagram of a 2-DOF dynamic model of CFP sliders. The cantilever is fixed such that there is no relative motion between the slider and the cantilever.

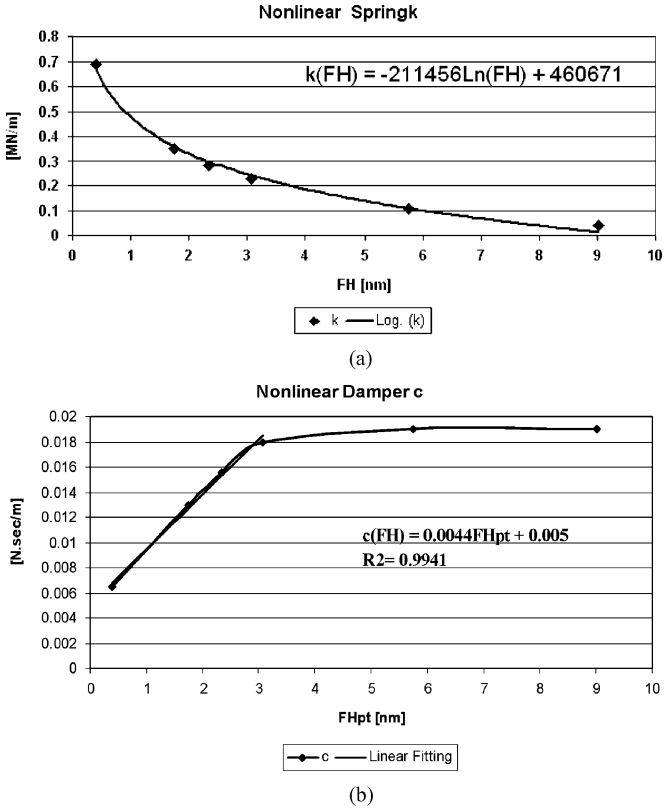

Fig. 9. (a) Nonlinear stiffness k and (b) nonlinear damping c as a function of FH at the PT.

respectively. The slider's mass M and moment of inertia I_θ are 1.6×10^{-6} kg and 2.2×10^{-13} kg·m^2, respectively. The parameters that need to be identified are described as follows: $k_{\rm l}$ and $k*$ are the air-bearing stiffnesses. $c_{\rm l}$ and $c*$ are the air-bearing damping coefficients. $d_{\rm l}$ and $d_{\rm t}$ are the distances from the resultant air-bearing force to the mass center of the slider. Index l or $*$ represents the value at the leading (two pads) or trailing edge (three pads).

A linear modal analysis program developed by CML [7], [8] is used to identify the parameters. The method uses impulse responses of the slider to obtain the air-bearing modal parameters, such as modal frequencies, damping ratios, mode shapes, and physical matrices (mass, stiffness, and damping). The impulse response is calculated here by using a constrained CML dynamic simulator, in which the slider's moment of inertia in the roll direction I_φ is increased to prohibit the slider from rolling and the linear disk velocity is 15 m/s. The initial impulse has to be extremely small to avoid any nonlinearity. The deflection of the cantilever is implemented in the CML dynamic simulator by setting the relative heights of the central trailing pad and the other four pads.

The two modal frequencies and two damping ratios (at FH $=$ 3 nm) were identified as 69 and 165 kHz, and 4.85% and 1.75%, respectively. The six parameters $k*, k_{\rm l}, c*, c_{\rm l}, d_{\rm t}$, and $d_{\rm l}$ were determined algebraically by equating the six elements in the matrices [c] and [k] and those identified by the linear modal analysis approach. It was observed that only $k*$ and $c*$ exhibit significant nonlinearities.

In the active mode of operation, the cantilever actuator is expected to deflect dynamically. Hence, the central trailing pad, located at the end of the cantilever, has relative motion with respect to the other two trailing pads. In that case, a more realistic model is shown in Fig. 8(b), where $k*$ and $c*$ are decomposed into two parts, resulting in four parameters $k_{\rm t}, c_{\rm t}, k$, and c · $k_{\rm t}$ and $c_{\rm t}$ are the air-bearing stiffness and damping coefficient for the two-side trailing pads of the slider body. k and c are the stiffness and damping for the central trailing pad, which is located at the end of the cantilever actuator. l (=0.595 mm) is the distance from the slider's mass center to the read/write transducer. Since the FH at the two-side trailing pads is usually more than 40 nm, the linearized values of $k_{\rm t}$ and $c_{\rm t}$ are used. The linearized values of $k_{\rm t}, k_{\rm l}, c_{\rm l}, d_{\rm l}$, and $d_{\rm t}$ are 3×10^5 N/m, 1.95×10^5 N/m, 0.04386 N·s/m, 0.2717 mm, and 0.5358 mm, respectively. k and c are the only nonlinear elements and $c_{\rm t}$ is set to zero for simplicity. Fig. 9(a) and (b) shows plots of k and c as functions of FH. A natural logarithm curve was found to be the best fit to the stiffness within the range of interest, giving a $k(\mathrm{FH_{pt}})$ in units of newton per meter as a function of FH at the PT$(\mathrm{FH_{pt}})$ in units of nanometers

$$k(\mathrm{FH_{pt}}) = \beta_{\rm k}\ \ln(\mathrm{FH_{pt}}) + \alpha_{\rm k} \tag{4}$$

where the coefficients $\beta_{\rm k}$ and $\alpha_{\rm k}$ for this fit are determined to be $-211\,456$ and 460 671, respectively.

The damping coefficient c is almost constant for FH between 3 and 9. A linear curve fit is applied to c for FH less than 3 nm, giving a c (FH) in units of newton-second per meter as a function of FH at the PT (FH) in units of nanometers

$$c(\mathrm{FH_{pt}}) = \beta_{\rm c}\mathrm{FH_{pt}} + \alpha_{\rm c} \tag{5}$$

where the coefficients $\beta_{\rm c}$ and $\alpha_{\rm c}$ for this fit are determined to be 0.0044 and 0.005, respectively.

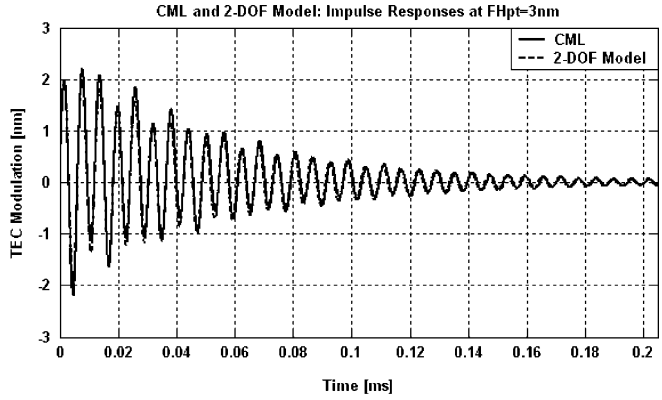

(a)

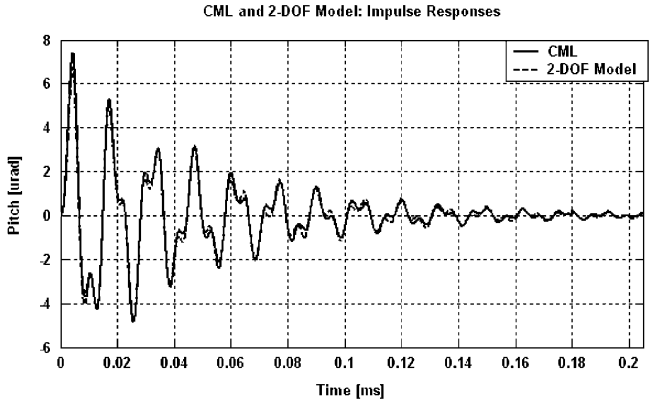

(b)

Fig. 10. Impulse responses (initial velocity 0.002 m/s in z-direction) of CFP slider simulated by the 2-DOF model and the CML dynamic simulator. (a) TEC FH modulation and (b) pitch modulation about the equilibrium of $\mathrm{FH} = 3.07$ nm.

The response predicted by this nonlinear 2-DOF model was compared with that of the CML dynamic simulator by computing the motion resulting from an impulse. The results for an FH of 3 nm are shown in Figs. 10 and 11 in both the time and the frequency (FFT) domains. H11 and H21 are the responses in the z_M-and θ-directions due to an impulse in the z_M-direction, respectively. As seen, there is good agreement between the 2-DOF model and the CML simulator.

C. Intermolecular and Electrostatic Forces

Due to the reduction in the spacing between the slider and the disk, the threshold for new nanoscale phenomena will be crossed. In particular, new forces between the slider and disk come into play, such as intermolecular and electrostatic forces. A study of the effects of intermolecular forces and electrostatic forces was presented by Gupta and Bogy [1]. The intermolecular and electrostatic forces do not have a significant effect on the flying characteristics of high flying sliders (spacings greater than 10 nm), but they become increasingly important at low spacings (below 5 nm). These forces are attractive in nature and hence result in a reduction in fly height as compared to what would be the case without them. Experimental investigations have indicated that these short-range forces are one of the major instability factors in ultralow HDI.

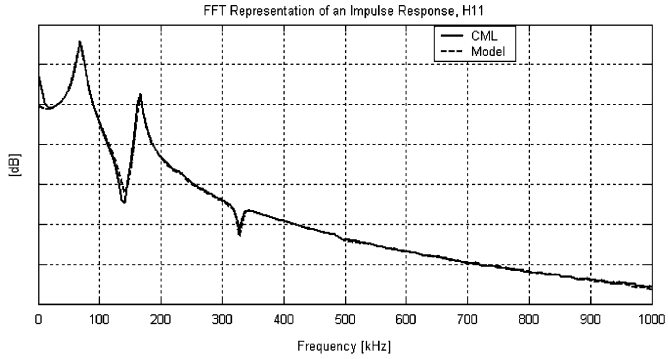

(a)

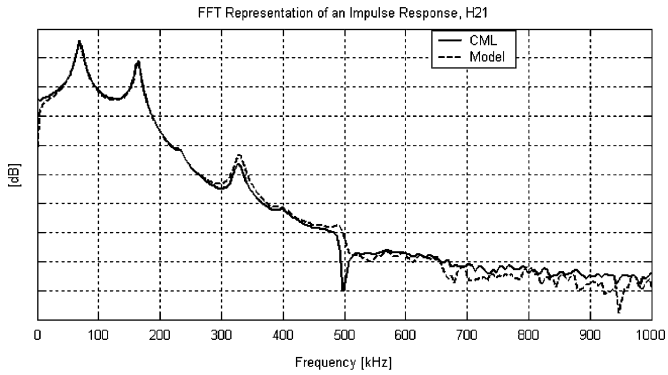

(b)

Fig. 11. Impulse responses (initial velocity 0.002 m/s in z-direction) of CFP slider simulated by the 2-DOF model and the CML dynamic simulator shown in the frequency (FFT) domains. (a) The response of TEC FH and (b) the response of pitch about the equilibrium of $\mathrm{FH} = 3.07$ nm.

These short-range attractive forces are considered to act on the cantilever tip, i.e., the 1-DOF cantilever actuator

$$F_{\mathrm{act}} = F_{\mathrm{imf}} + F_{\mathrm{elec}}$$

where

$$F_{\mathrm{imf}} = -\frac{A'}{(\mathrm{FH_{pt}})^3} + \frac{B'}{(\mathrm{FH_{pt}})^9} \tag{6}$$

$$F_{\mathrm{elec}} = -\frac{1}{2}\varepsilon_0 k_{\mathrm{e}} A_{\mathrm{eq}} \frac{V^2}{(\mathrm{FH_{pt}})^2} \tag{7}$$

and where the constants $A'(1.8 \times 10^{-30})$ and $B'(2.7 \times 10^{-88})$ depend on the ABS design and material properties of the slider and disk. In this paper, the values given by Thornton [11] are used. The electrostatic force due to the electrical potential across the slider and disk is shown in (7). ε_o, k_e, and V are the permittivity constant (8.85×10^{-12} F/m), dielectric constant of the medium (1 for air), and the potential difference between the slider and the disk. The area constant A_{eq} in (7) is chosen such that the force agrees with that simulated by the CML static simulator. A comparison of the electrostatic forces between the CML simulator and the model is shown in Fig. 12.

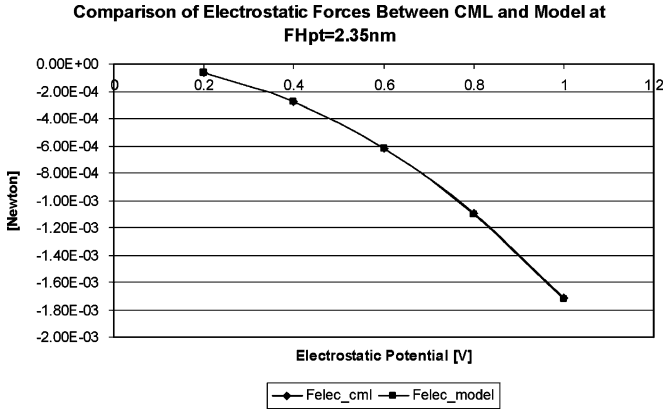

Fig. 12. Comparison of electrostatic forces between CML simulator and model. The forces are calculated when the slider is fixed at $\mathrm{FH_{pt}} = 2.35$ nm and pitch $= 221$ μrad.

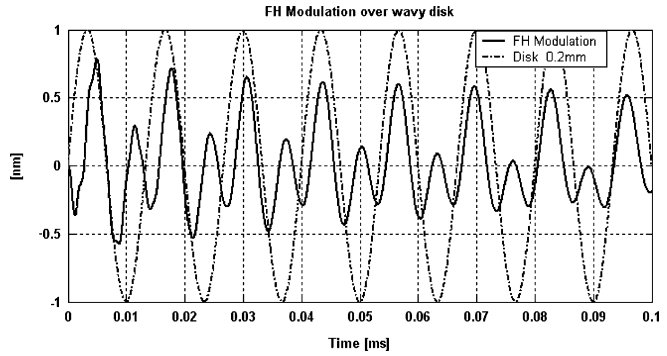

Fig. 13. FHM of 3-DOF over a wavy disk surface (wavelength is 0.2 mm) without short-range forces.

D. Nonlinear 3-DOF-Lumped Model of CFP Sliders

Based on the analysis in Sections III-A–III-C, a nonlinear 3-DOF model was constructed as shown in Fig. 4 and the equation of motion is as follows:

$$[m]\{\ddot{x}\} + [c]\{\dot{x}\} + [k]\{x\} = \{F\} \tag{8}$$

where

$$\{x\} = \begin{bmatrix} z_M \\ \theta \\ z_{\mathrm{m}} \end{bmatrix}, \quad [m] = \begin{bmatrix} M & 0 & 0 \\ 0 & I_\theta & 0 \\ 0 & 0 & m \end{bmatrix}$$

$$[c] = \begin{bmatrix} c_{\mathrm{t}} + c_{\mathrm{l}} + c_{\mathrm{c}} & -(d_{\mathrm{t}}c_{\mathrm{t}} - d_{\mathrm{l}}c_{\mathrm{l}} - lc_{\mathrm{c}}) & -c_{\mathrm{c}} \\ -(d_{\mathrm{t}}c_{\mathrm{t}} - d_{\mathrm{l}}c_{\mathrm{l}} - lc_{\mathrm{c}}) & d_{\mathrm{t}}^2 c_{\mathrm{t}} + d_{\mathrm{l}}^2 c_{\mathrm{l}} + d_{\mathrm{c}}^2 c_{\mathrm{c}} & lc_{\mathrm{c}} \\ -c_{\mathrm{c}} & lc_{\mathrm{c}} & c + c_{\mathrm{c}} \end{bmatrix}$$

$$[k] = \begin{bmatrix} k_{\mathrm{t}} + k_{\mathrm{l}} + k_{\mathrm{c}} & -(d_{\mathrm{t}}k_{\mathrm{t}} - d_{\mathrm{l}}k_{\mathrm{l}} - lk_{\mathrm{c}}) & -k_{\mathrm{c}} \\ -(d_{\mathrm{t}}k_{\mathrm{t}} - d_{\mathrm{l}}k_{\mathrm{l}} - lk_{\mathrm{c}}) & d_{\mathrm{t}}^2 k_{\mathrm{t}} + d_{\mathrm{l}}^2 k_{\mathrm{l}} + d_{\mathrm{c}}^2 k_{\mathrm{c}} & lk_{\mathrm{c}} \\ -k_{\mathrm{c}} & lk_{\mathrm{c}} & k + k_{\mathrm{c}} \end{bmatrix}$$

$$\{F\} = \begin{bmatrix} f_{\mathrm{dt}} + f_{\mathrm{dl}} \\ d_{\mathrm{l}} f_{\mathrm{dl}} - d_{\mathrm{t}} f_{\mathrm{dt}} \\ F_{\mathrm{act}} - u + f_{\mathrm{d}} \end{bmatrix}$$

$$= \begin{bmatrix} k_{\mathrm{t}} z_{\mathrm{dt}} + c_{\mathrm{t}} \dot{z}_{\mathrm{dt}} + k_{\mathrm{l}} z_{\mathrm{dl}} + c_{\mathrm{l}} \dot{z}_{\mathrm{dl}} \\ -d_{\mathrm{t}}(k_{\mathrm{t}} z_{\mathrm{dt}} + c_{\mathrm{t}} \dot{z}_{\mathrm{dt}}) + d_{\mathrm{l}}(k_{\mathrm{l}} z_{\mathrm{dl}} + c_{\mathrm{l}} \dot{z}_{\mathrm{dl}}) \\ F_{\mathrm{act}} - u + (k z_{\mathrm{d}} + c \dot{z}_{\mathrm{d}}) \end{bmatrix}.$$

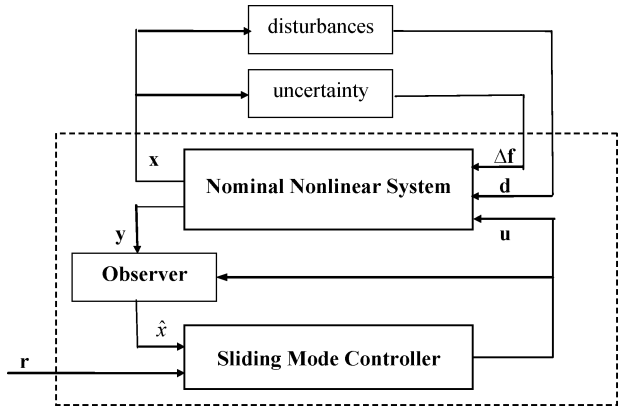

Fig. 14. Framework of observer-based sliding mode controller.

Note that the disk profile quantities $z_{\mathrm{dt}}, z_{\mathrm{dl}}$, and z_d are assumed unknown but bounded.

Numerical simulations were conducted to calculate the responses of the system over a harmonic wavy disk. The cantilever actuator was deflected to achieve an FH of 2.35 nm. The peak-to-peak amplitude of the waviness is assumed to be 2 nm, and the waviness wavelength is 0.2 mm, corresponding to a frequency of 75 kHz at a linear disk velocity of 15 m/s. The FHM is obtained by subtracting z_{d} from z_{m}. Fig. 13 shows the responses without including the short-range forces. However, when the forces are included in the model, severe contacts were indicated and the slider could not fly stably.

IV. Design of Nonlinear Compensators

The short-range forces and disk waviness cause instability of the HDI and increase the FHM. It is desirable to compensate the forces and to suppress the modulation by feedback control. Because of the nonlinear components and uncertain disturbance in the air-bearing systems, an observer-based nonlinear control or nonlinear compensator design approach is used [9]. The schematic diagram of the controller is shown in Fig. 14. Assuming that the real-time FH can be measured, we first built an observer for the state estimation and designed a sliding control law using the observer as the plant.

Equation (8) is transformed into a state-space representation as follows:

$$\begin{cases} \dot{x} = Ax + Bu + f(x) + f_{\mathrm{d}} \\ y = Cx \end{cases}. \tag{9}$$

The control goal is to push the FHM to zero. If z_{m} is used as a state, this will be a tracking problem, $z_{\mathrm{m}} \to z_{\mathrm{d}}$. However, the future z_{d} is unknown. To resolve this, a new state z is defined as

$$z = z_{\mathrm{m}} - z_{\mathrm{d}}.$$

The states of the system are discussed in the equation shown at the bottom of the page.

The observer is designed as

$$\dot{\hat{x}} = A\hat{x} + Bu + f(\hat{x}) + L(y - C\hat{x}). \tag{10}$$

The error dynamic is obtained by subtracting $\dot{x}$ from $\dot{\hat{x}}$

$$\dot{\tilde{x}} = \dot{\hat{x}} - \dot{x} = (A - LC)\tilde{x} - f_{\mathrm{d}}. \tag{11}$$

Note that $\boldsymbol{f}(\cdot)$ and $\boldsymbol{f_{\mathrm{d}}}$ represent the nonlinear force components and disturbances, respectively. The observer gain matrix $\boldsymbol{L}$ is chosen as in a Luenberger observer [12] so as to place the poles of $(\boldsymbol{A} - \boldsymbol{L}C)$ at desired locations.

The sliding surface is defined as

$$s = \dot{\hat{x}}_5 + \lambda \hat{x}_5. \tag{12}$$

We then have

$$\begin{aligned}\dot{s} &= \dot{\hat{x}}_6 + \lambda \dot{\hat{x}}_5 \\ &= \frac{1}{m}[k_{\mathrm{c}}\hat{x}_1 + c_{\mathrm{c}}\hat{x}_2 - lk_{\mathrm{c}}\hat{x}_3 - lc_{\mathrm{c}}\hat{x}_4 - (k + k_{\mathrm{c}})\hat{x}_5 \\ &\quad - (c + c_{\mathrm{c}})\hat{x}_6 + F_{\mathrm{act}} - u] + L_6(x_5 - \hat{x}_5) \\ &\quad + \lambda[\hat{x}_6 + L_5(x_5 - \hat{x}_5)].\end{aligned} \tag{13}$$

The control law is designed as

$$\begin{aligned}u &= k_{\mathrm{c}}\hat{x}_1 + c_{\mathrm{c}}\hat{x}_2 - lk_{\mathrm{c}}\hat{x}_3 - lc_{\mathrm{c}}\hat{x}_4 - (k + k_{\mathrm{c}})\hat{x}_5 \\ &\quad - (c + c_{\mathrm{c}})\hat{x}_6 + F_{\mathrm{act}} + m\lambda[\hat{x}_6 + L_5(x_5 - \hat{x}_5)] \\ &\quad + mL_6(x_5 - \hat{x}_5) + m\eta s\end{aligned} \tag{14}$$

such that

$$\dot{s}s = -\eta s^2 < 0. \tag{15}$$

Equation (15) guarantees that s approaches zero based on Lyapunov theory and drives the estimated FHM $\hat{x}_5$ to zero exponentially according to (12).

To investigate the controller's performance, we conducted a large number of numerical simulation experiments. Fig. 15(a) shows that the FHM can be effectively suppressed even with the intermolecular force and an electrostatic potential of 0.5 V between the disk and slider (which is an unstable system without control). The applied control voltage and the cantilever deflection are also shown in Fig. 15(b) and (c), respectively. The observer performance is demonstrated by the comparison of the estimated and true FHM in Fig. 16 where it is seen that the error between the true and estimated values is very small.

When the electrostatic potential between the slider and disk increases from 0 to 1 V (i.e., electrostatic forces increase), the mean control voltage shifts from 0 to about 3.3 V to compensate the increased electrostatic forces, as shown in Fig. 17. This dc shift can actually decrease the applied dc control voltage required to bring the cantilever into the active operational mode.

V. Conclusion

Due to the effects of short-range forces and disk morphology, it is unlikely that a passive air-bearing slider will be able to form a reliable head-disk interface at a spacing much less than 5 nm. Substantial research has been carried out on contact recording, in which the slider is expected to be in full contact with the disk.

$$x=[x_1 \quad x_2 \quad x_3 \quad x_4 \quad x_5 \quad x_6]^T = [z_M \quad \dot{z}_M \quad \theta \quad \dot{\theta} \quad z \quad \dot{z}]^T$$

$$A=\begin{bmatrix} 0 & 1 & 0 & 0 & 0 & 0 \\ -\frac{1}{M}(k_{\mathrm{t}}+k_{\mathrm{l}}+k_{\mathrm{c}}) & -\frac{1}{M}(c_{\mathrm{t}}+c_{\mathrm{l}}+c_{\mathrm{c}}) & -\frac{1}{M}(-d_{\mathrm{t}}k_{\mathrm{t}}+d_{\mathrm{l}}k_{\mathrm{l}}-lk_{\mathrm{c}}) & -\frac{1}{M}(-d_{\mathrm{t}}c_{\mathrm{t}}+d_{\mathrm{l}}c_{\mathrm{l}}-lc_{\mathrm{c}}) & \frac{k_{\mathrm{c}}}{M} & \frac{c_{\mathrm{c}}}{M} \\ 0 & 0 & 0 & 1 & 0 & 0 \\ -\frac{1}{I}(-d_{\mathrm{t}}k_{\mathrm{t}}+d_{\mathrm{l}}k_{\mathrm{l}}-lk_{\mathrm{c}}) & -\frac{1}{I}(-d_{\mathrm{t}}c_{\mathrm{t}}+d_{\mathrm{l}}c_{\mathrm{l}}-lc_{\mathrm{c}}) & -\frac{1}{I}\left(d_{\mathrm{t}}^2k_{\mathrm{t}}+d_{\mathrm{l}}^2k_{\mathrm{l}}+l^2k_{\mathrm{c}}\right) & -\frac{1}{I}\left(d_{\mathrm{r}}^2c_{\mathrm{r}}+d_{\mathrm{f}}^2c_{\mathrm{f}}+l^2c_{\mathrm{c}}\right) & -\frac{lk_{\mathrm{c}}}{I} & -\frac{lc_{\mathrm{c}}}{I} \\ 0 & 0 & 0 & 0 & 0 & 1 \\ \frac{k_{\mathrm{c}}}{m} & \frac{c_{\mathrm{c}}}{m} & -\frac{lk_{\mathrm{c}}}{m} & -\frac{lc_{\mathrm{c}}}{m} & -\frac{(k+k_{\mathrm{c}})}{m} & -\frac{(c+c_{\mathrm{c}})}{m} \end{bmatrix}$$

$$B=[0 \quad 0 \quad 0 \quad 0 \quad 0 \quad -\frac{1}{m}]^T$$

$$C=[0 \quad 0 \quad 0 \quad 0 \quad 1 \quad 0]$$

$$f(x)=\begin{bmatrix} 0 & 0 & 0 & 0 & 0 & \frac{1}{m}F_{\mathrm{act}} \end{bmatrix}^T$$

$$f_d=\begin{bmatrix} 0 \\ k_{\mathrm{c}}z_{\mathrm{d}}+c_{\mathrm{c}}\dot{z}_{\mathrm{d}}+\frac{1}{M}(k_{\mathrm{t}}z_{\mathrm{dt}}+c_{\mathrm{t}}\dot{z}_{\mathrm{dt}}+k_{\mathrm{l}}z_{\mathrm{dl}}+c_{\mathrm{l}}\dot{z}_{\mathrm{dl}}) \\ 0 \\ -lk_{\mathrm{c}}z_{\mathrm{d}}-lc_{\mathrm{c}}\dot{z}_{\mathrm{d}}+\frac{d_{\mathrm{l}}}{I}(k_{\mathrm{l}}z_{\mathrm{dl}}+c_{\mathrm{l}}\dot{z}_{\mathrm{dl}})-\frac{d_{\mathrm{t}}}{I}(k_{\mathrm{t}}z_{\mathrm{dt}}+c_{\mathrm{t}}\dot{z}_{\mathrm{dt}}) \\ 0 \\ -\ddot{z}_{\mathrm{d}}-\frac{1}{m}(k_{\mathrm{c}}z_{\mathrm{d}}+c_{\mathrm{c}}\dot{z}_{\mathrm{d}}) \end{bmatrix}.$$

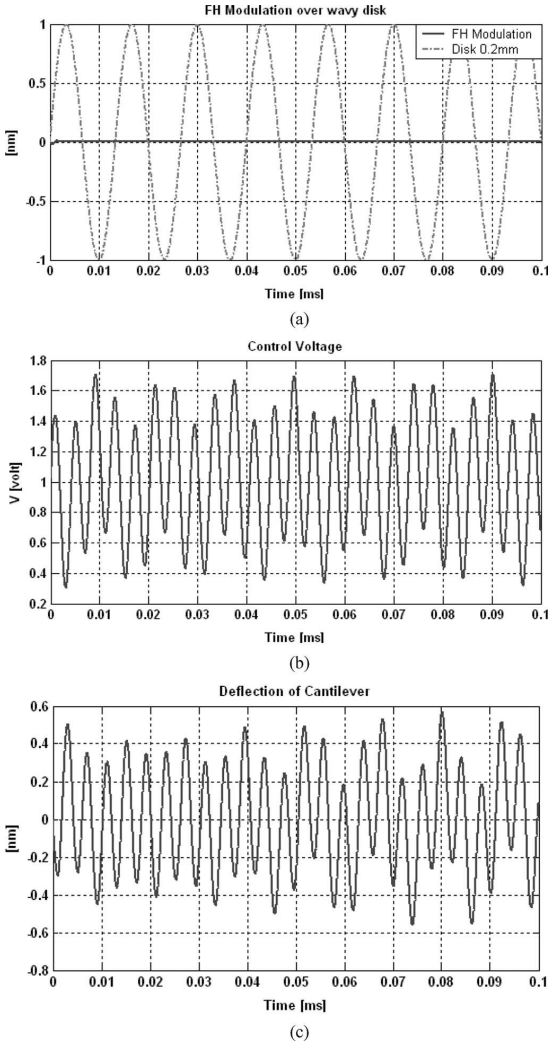

Fig. 15. (a) Results of FHM suppression of the CFP slider in the presence of intermolecular and electrostatic forces (0.5 V). The disk waviness wavelength is 0.2 mm. (b) Control voltage and (c) History of the cantilever deflection.

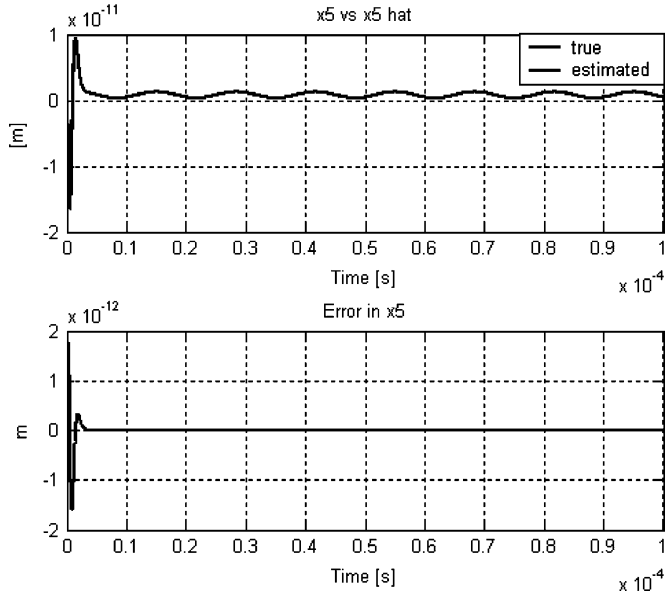

Fig. 16. True and estimated $\mathrm{FHM}(\times 5)$.

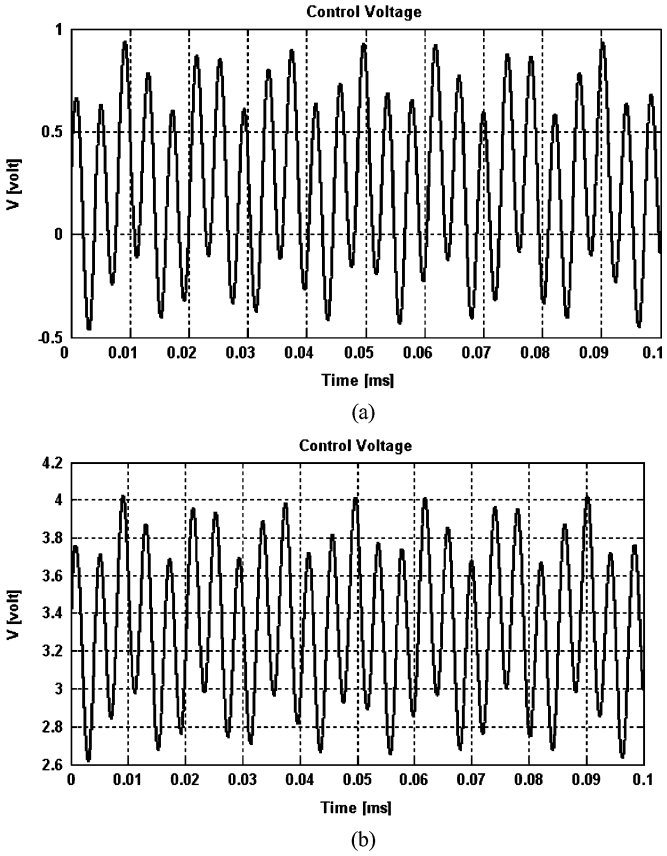

Fig. 17. Control voltages for different electrostatic potentials. The disk waviness wavelength is 0.2 mm. The electrostatic potentials between the slider and disk are (a) 0 V and (b) 1 V.

Several design considerations have been given in the literature, but it is still unclear how to implement such systems, namely the ABS design, the selection of lubricant, and protective overcoat.

In this paper, a new 3-DOF dynamic model is proposed for a CFP slider, which is actuated by a layer of piezoelectric material. A linear modal analysis is used to identify the air-bearing parameters. Good agreement is obtained for the air-bearing dynamics between the model and the CML dynamic simulator. An observer-based nonlinear sliding mode controller is designed based on the model. Numerical studies show that an FH below 3 nm is achieved and the FHM due to disk waviness is effectively reduced in the presence of short-range attractive forces.

REFERENCES

[1] V. Gupta and D. B. Bogy, "Dynamics of sub-5nm air bearing sliders in the presence of electrostatic and intermolecular forces at the head disk interface," *IEEE Trans. Magn.*, vol. 41, no. 2, pp. 610–615, Feb. 2005.

[2] M. Kurita and K. Suzuki, "Flying-height adjustment technologies of magnetic head sliders," *IEEE Trans. Magn.*, vol. 40, no. 1, pt. 2, pp. 332–336, Jan. 2004.

[3] M. Kurita, R. Tsuchiyama, M. Tokuyama, J. Xu, Y. Yoshimura, H. Kohira, L. Z. Su, and K. Kato, "Flying-height adjustment of a magnetic head slider with a piezoelectric micro-actuator," in *Proc. INTERMAG. Conf.*, Boston, MA, 2003, pp. GP–06.

[4] N. Tagawa, K. Kitamura, and A. Mori, "Design and fabrication of MEMS-based active sliders using double-layered composite PZT thin films in hard disk drives," *IEEE Trans. Magn.*, vol. 39, no. 2, pt. 2, pp. 926–931, Mar. 2003.

[5] A. Li, X. Liu, W. Clegg, D. F. L. Jenkins, and T. Donnelly, "Real-time method to measure head disk spacing variation under vibration conditions," *IEEE Trans. Instrum. Meas.*, vol. 52, no. 3, pp. 916–920, Jun. 2003.
[6] X. Liu, A. Li, W. Clegg, D. F. L. Jenkins, and P. Davey, "Head-disk spacing variation suppression via active flying height control," *IEEE Trans. Instrum. Meas.*, vol. 51, no. 5, pp. 897–901, Oct. 2002.
[7] Q. H. Zeng, L. S. Chen, and D. B. Bogy, "A modal analysis method for slider-air bearings in hard disk drives," Comput. Mechanics Lab., Dept. Mech. Eng., Univ. California at Berkeley, Tech. Rep. No. 96-021, 1996.
[8] Q. H. Zeng and D. B. Bogy, "The CML slider-air bearing parameter identification program," Comput. Mechanics Lab., Dept. Mech. Eng., Univ. California at Berkeley, Tech. Rep. No. 97-006, 1997.
[9] B. Song and J. K. Hedrick, "Observer-based dynamic surface control for Lipschitz nonlinear systems," in *Proc. 42nd IEEE Int. Conf. Decision Control*, vol. 1, Piscataway, NJ, Dec.2003, pp. 874–879.
[10] J. G. Smits and W.-S. Choi, "The constituent equations of piezoelectric heterogeneous bimorphs," *IEEE Trans. Ultrason., Ferroelect., Freq. Control*, vol. 38, no. 3, pp. 256–270, May 1991.
[11] B. H. Thornton and D. B. Bogy, "A parametric study of head-disk interface instability due to intermolecular forces," *IEEE Trans. Magn.*, vol. 40, no. 1, pt. 2, pp. 337–344, Jan. 2004.
[12] K. Ogata, *State Space Analysis of Control Systems*. Englewood Cliffs, NJ: Prentice-Hall, 1967.

Jia-Yang Juang (S'05) received the B.S. and M.S. degrees from National Taiwan University, Taipei, Taiwan, R.O.C., in 1997 and 1999, respectively, both in mechanical engineering. He is currently pursuing the Ph.D. degree at the University of California, Berkeley, in mechanical engineering.

His research interests are the applications of nanotechnology, MEMS, and control engineering to ultrahigh density information storage.

Mr. Juang is a student member of the American Society of Mechanical Engineers.

David B. Bogy (M'91–SM'92–F'01) received the B.S. degree in geology and mechanical engineering and the M.S. degree in mechanical engineering from Rice University, Houston, TX, in 1959 and 1961, respectively, and the Ph.D. degree in applied mathematics from Brown University, Providence, RI, in 1966.

He was a Postdoctoral Fellow in applied mechanics at the California Institute of Technology. In 1967, he joined the faculty of the Department of Mechanical Engineering, University of California, Berkeley. From 1991 to 1999, he was the Chairman of the Department of Mechanical Engineering, University of California. He is also the founding Director of the Computer Mechanics Laboratory, Department of Mechanical Engineering.

Dr. Bogy is a Fellow of the American Academy of Mechanics and the American Society of Mechanical Engineers. He is the William S. Floyd, Jr. Distinguished Professor in Engineering. He serves on the U.S. National Committee on Theoretical and Applied Mechanics. He has served as the Chair of the Executive Committees of the Applied Mechanics and the Tribology Divisions of the American Society of Mechanical Engineers. He was the recipient of the ASME Tribology Division Mayo D. Hersey Award in 1999. He is a member of the National Academy of Engineers.